

Article

Influence of Overheating on High-Cycle Fatigue Characteristics of the Base Metal and Weld Metal of Low-Carbon Steel Welded Joints

Sergey A. Nikulin ¹, Stanislav O. Rogachev ^{1,2,*} , Dmitriy V. Prosvirnin ² , Svetlana V. Pivovarchik ², Vladislav A. Belov ¹, Nikolay V. Shplis ¹, Mikhail Y. Zadorozhnyy ^{3,4} and Vladimir M. Khatkevich ¹

¹ Department of Physical Metallurgy and Physics of Strength, National University of Science and Technology MISIS, 119049 Moscow, Russia; nikulin@misis.ru (S.A.N.); vbelov@yandex.ru (V.A.B.); shplisnikolay@mail.ru (N.V.S.); hatvm87@mail.ru (V.M.K.)

² Baikov Institute of Metallurgy and Materials Science, Russian Academy of Sciences, 119334 Moscow, Russia; imetran@yandex.ru (D.V.P.); pivovarchiksv@yandex.ru (S.V.P.)

³ Center for Project Activities, Moscow Polytechnic University, 107023 Moscow, Russia; m.y.zadorozhnyj@mospolytech.ru

⁴ Research Centre of Composite Materials, National University of Science and Technology MISIS, 119049 Moscow, Russia

* Correspondence: csaap@mail.ru; Tel.: +7-903-967-5782

Abstract: The results of a high-cycle fatigue testing of our samples were obtained, and a comparative assessment of the properties of the base metal and weld metal of 09G2S-type steel (13Mn6 according to the DIN17145-80 standard) before and after overheating (1200 °C, 3.7 h) was performed. The welded joints between the sheets of 09G2S steel were obtained through automatic argon arc welding. The fatigue tests were carried out under repeated tensile loading. The “maximum cycle stress—number of cycles to failure” fatigue curves of the samples were plotted. The fracture surfaces of the samples were studied, and the fatigue failure mechanisms were analyzed. It was shown that, during testing, all samples demonstrated cyclic hardening behavior. The samples of the base metal as delivered had the highest endurance limit, and the smallest endurance limit was found in the samples of the base metal and weld metal after overheating, the endurance limits of which were similar. The fracture mechanism of all samples was quasi-brittle with the presence of very thin fatigue micro-grooves. The final rupture of all samples had a ductile dimple type.

Keywords: low-carbon low-alloy steel; microstructure; overheating; high-cycle fatigue; cyclic hardening; fractography



Citation: Nikulin, S.A.; Rogachev, S.O.; Prosvirnin, D.V.; Pivovarchik, S.V.; Belov, V.A.; Shplis, N.V.; Zadorozhnyy, M.Y.; Khatkevich, V.M. Influence of Overheating on High-Cycle Fatigue Characteristics of the Base Metal and Weld Metal of Low-Carbon Steel Welded Joints. *Metals* **2023**, *13*, 1707. <https://doi.org/10.3390/met13101707>

Academic Editors: Alberto Campagnolo and Alberto Sapora

Received: 31 July 2023

Revised: 22 September 2023

Accepted: 26 September 2023

Published: 7 October 2023



Copyright: © 2023 by the authors. Licensee MDPI, Basel, Switzerland. This article is an open access article distributed under the terms and conditions of the Creative Commons Attribution (CC BY) license (<https://creativecommons.org/licenses/by/4.0/>).

1. Introduction

Low-carbon, low-alloy steels of the 09G2S type (13Mn6 according to the DIN17145-80 standard [1]) have a combination of satisfactory mechanical properties, good weldability, and a low cost, which make them important structural materials for the manufacturing of various large metal constructions in the chemical, oil-refining, shipbuilding, and energy industries, as well as in other fields [2–5]. In particular, 09G2S steel is widely used in the production of pipes for transporting various liquids (water, oil, etc.), tanks for various purposes, steam boilers, etc. [6,7].

In emergency situations, the ambient temperature can differ significantly from the nominal operating temperature of the metal construction [8]. Thus, a severe accident beyond the design basis at a nuclear power plant is associated with the destruction of the reactor vessel and melting of the core. To block the exit of the corium beyond the tight enclosure, a melt localization device or a so-called core catcher vessel (CC vessel) is provided, the main structural elements of which are composed of 09G2S steel [9]. According to calculations, the temperature of the corium entering the CC vessel exceeds several

thousand degrees, and the CC vessel itself, in the process of the localization and cooling of the corium melt, is heated to temperatures of about 1200 °C [10,11]. The prolonged thermal exposure causes a significant change in the structure of the metal and, as a consequence, causes the degradation of its mechanical properties. To calculate the minimum required margin of safety for a metal construction in emergency conditions, it is important to know the effects of extreme temperatures and force conditions on the mechanical properties of the material. Such data are available in the literature, but they mainly concern the static strength and impact strength [12,13]. At the same time, the most important property of a structural material is its fatigue strength. This is especially true for CC vessel construction conducted in areas with increased seismic hazards. The fatigue characteristics of low-carbon steels have been extensively studied [14–21]. In particular, the mechanisms of fatigue crack propagation [22], the relationship between the fatigue groove spacing and the fatigue crack propagation rate [23], and the effect of the chemical composition [24] have been studied. There are papers in which the effect of aging on the fatigue characteristics has been studied, in which it was shown that the long-term (15-year) natural aging of 20-type carbon steel (0.2% C) causes an increase in the static strength but at the same time reduces the fatigue strength by 1.6 times; in addition, it was found that the endurance of samples at the stage of damage accumulation was much less than at the stage of nucleation and during the growth of macro-cracks [25]. Kim Y. et al. observed the transition of the fatigue failure regime from a high cycle to an extremely low cycle when increasing the amplitude of the deformation of the samples of a base metal and a welded joint (plasma arc welding) made of low-carbon steel (0.1% C; 0.7% Mn) with a ferrite–pearlite microstructure [14]. It has been established that the base metal in a high-cycle fatigue mode demonstrates initial cyclic softening followed by cyclic stabilization, while the welded joint fails in an extremely low-cycle fatigue mode without the cyclic stabilization of the initial cyclic softening.

A number of works have been devoted to predicting the fatigue life of metal structures, which is of utmost importance in the design of engineering components, especially in those containing defects (or notches) [26,27]. It has been established that the result of a probabilistic fatigue analysis of metal depends on both the effect of size and defect location. In addition, the superiority of a surface defect over an internal one in the initiation of fatigue failure has once again been noted.

At the same time, little attention has been paid to the study of the fatigue of low-carbon steels, and especially welds, after extreme thermal effects that are typical in emergency situations. Although fatigue strength characteristics are not directly used for strength analyses and in the structural design of CC vessels, the fatigue life is the most important characteristic of any structural material. Therefore, these data are necessary from the point of view of guaranteeing the reliability of CC vessel construction. An analysis of the few available research results on this issue is difficult to perform due to the fact that many factors affect the fatigue strength characteristics: the specimen type, the structure of the material, the quality of the surface, the loading mode during testing, other test conditions, etc. In the case of a welded joint, another influencing factor appears, namely the welding method. In addition, researchers use different approaches to assess fatigue strength [14,18,25]. Therefore, designers often require fatigue test data for a particular material that take into account its operating conditions.

In this study, comparative studies on the high-cycle fatigue of the base metal and the weld metal of 09G2S low-carbon steel, as delivered and after overheating, were carried out while simulating the conditions of severe accidents at nuclear power plants. The data obtained are necessary to guarantee the safe and reliable operation of CC vessel construction, especially in seismically active regions.

2. Materials and Methods

2.1. Materials

09G2S steel (13Mn6 according to the DIN17145-80 standard [1]) was obtained for the research as delivered (a 60 mm thick sheet after quenching and low tempering). The welded joints between the steel sheets were obtained through automatic argon arc welding without preheating the materials to be joined. A 2 mm diameter SV-08G2S welding wire was used, the chemical composition of which was close to 09G2S steel. The welding parameters were as follows: a welding speed of about 1 mm/s, a wire feed speed of 5 mm/s, a current of 190–210 A, and an arc voltage of 9–10 V. The chemical compositions of the base metal and the weld metal, determined using the optical emission method, did not differ significantly (see Table 1).

Table 1. Chemical composition (wt.%) of 09G2S steel welded joint.

Material	Fe	C	Si	Mn	P	S	Cr	Ni	Cu	Co
Base metal	Bal.	0.10	0.67	1.54	0.012	0.005	0.07	0.12	0.15	0.02
Weld metal	Bal.	0.09	0.61	1.49	0.012	0.005	0.04	0.07	0.10	0.01
13Mn6	Bal.	<0.12	0.5–0.8	1.3–1.7	<0.03	<0.04	<0.3	<0.3	<0.3	-

The studies were carried out using samples of the base metal and weld metal taken under two conditions:

1. As delivered;
2. After overheating: heating up to 1200 °C at a rate of 200 °C/h; exposure for 3.7 h; and further cooling in the furnace to room temperature.

The heat treatment was carried out in an electric furnace of the SNVE 1.3.1/16I4 type in a vacuum of $\sim 6.5 \times 10^{-3}$ Pa.

2.2. Methods

The static mechanical properties at room temperature were determined using a Zwick/Roell machine with a gripper speed of 5 mm/min. We used circular cross-section specimens with a threaded fastening and with a length and diameter for the gauge part of 20 mm and 4 mm, respectively, which were created using turning equipment (Figure 1a). Three specimens were tested for each condition of metal.

High-cycle fatigue tests at room temperature were carried out under repeated tension conditions with a cycle asymmetry coefficient $R = 0.1$ (the ratio of the minimum cycle stress to the maximum one) using an Instron Electropuls E3000 testing machine at a frequency of 30 Hz according to GOST 25.502-79 (a Russian document [28]). Flat specimens were used, which were cut using the electrical discharge machining method (Figure 1b). Each specimen was cut so that its working part corresponded directly to the weld (the central zone of the welded joint). The entire surface of the specimens was subjected to mechanical polishing for a mirror finish. The installation and fixing of the specimens in the testing machine did not cause additional stresses from the beating and misalignment of the specimens and grips. The total error in loading the specimens during testing did not exceed 0.25% of the value of the specified loads. Three fatigue specimens were tested for each stress level.

The analysis of fatigue fractures in the specimens was carried out using a TESCAN VEGA Compact scanning electron microscope (TESCAN, Brno, Czech Republic) at $\times 80$ – $\times 5000$ magnification. A quantitative analysis of fatigue fractures (fatigue fracture area and fatigue groove spacing) was carried out in the Image Expert software (ImageExpert Pro 3, NEXYS, Moscow, Russia) environment.

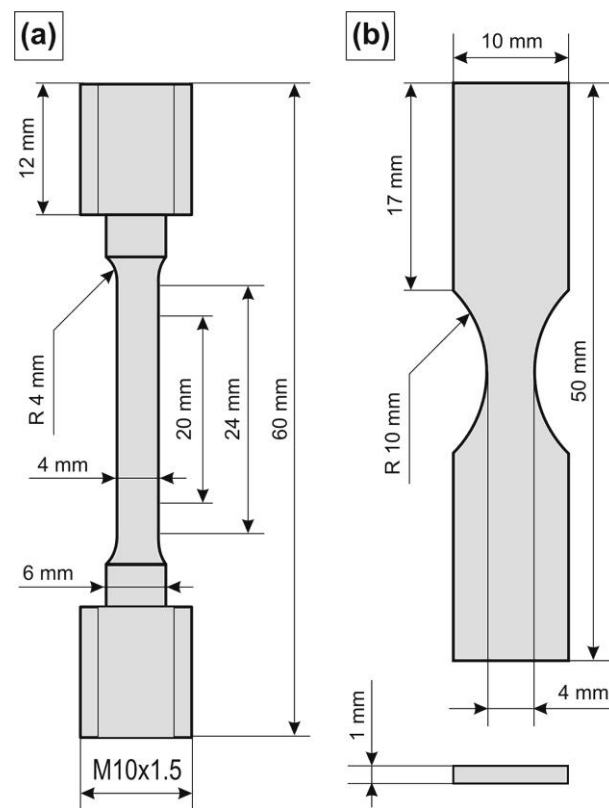


Figure 1. Specimens' dimensions for (a) static and (b) cyclic tests.

The Vickers microhardness profiles across the welded joint with a 1 mm step were measured using a MICROMET 5101 tester (Buehler, Wooster, OH, USA) at a load of 300 g.

The microstructure was studied using an NIM-100 optical microscope (LOMO, St. Petersburg, Russia) at $\times 200$ magnification after etching sections in a 5% solution of nitric acid in ethanol. In addition, the surface of the gauge part of the specimens after the fatigue tests was studied.

Electron microscopic studies were performed using a JEM-2100 JEOL transmission microscope (JEOL Ltd., Tokyo, Japan) with an EDS analyzer. X-ray spectral microanalyses of the structure and the plotting of concentration maps were carried out using a JEM-2100Plus JEOL (JEOL Ltd., Tokyo, Japan) transmission microscope equipped with a BRUKER XFlash 6TI60 analyzer (Bruker, Billerica, MA, USA).

3. Results

3.1. Microstructure

Figure 2 shows the OM images of the microstructure of the 09G2S steel samples under four conditions. The as-delivered base metal and weld samples (after quenching and tempering) had a similar fine microstructure with a large extent of the boundaries of the structure components (Figure 2a,c). Quenching and subsequent tempering led to the formation of quasi-polygonal ferrite that was practically free from carbide precipitates as well as fine-grained decomposition products of lower bainite with a higher content of fine cementite, which is typical for low-carbon steels [29]. The size of the former austenite grain in the base metal and in the weld metal as delivered did not differ significantly and amounted to 27 and 32 μm , respectively [13].

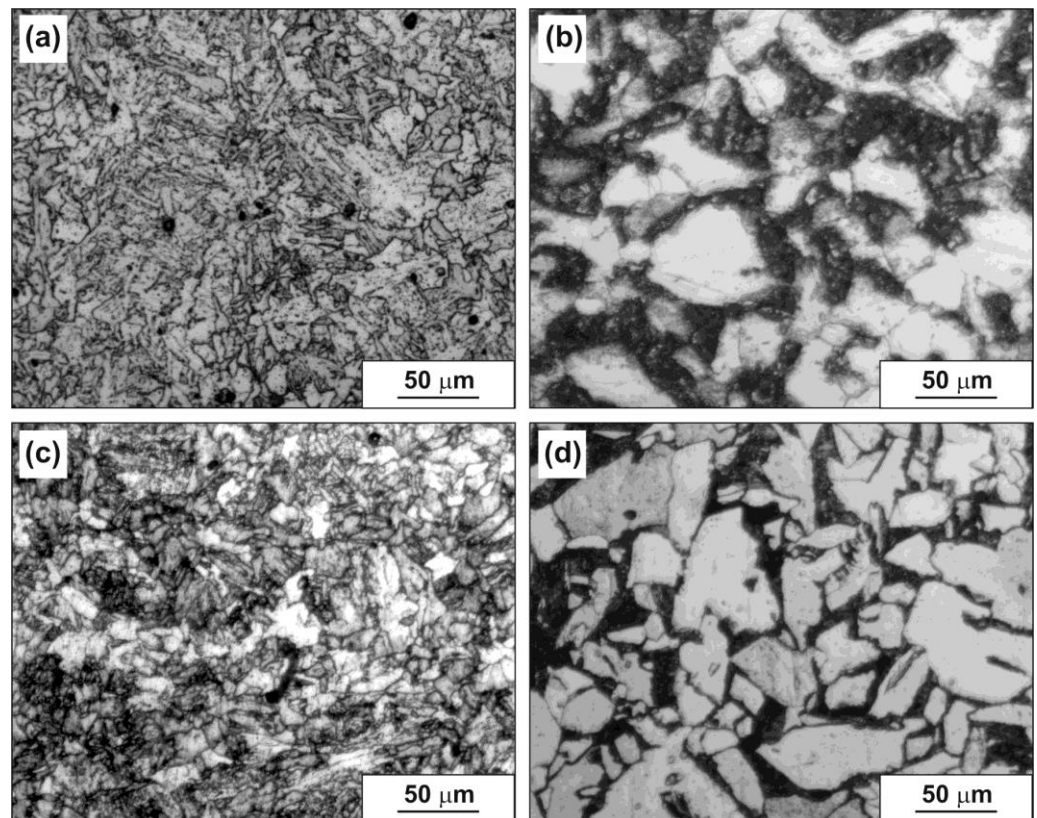


Figure 2. OM microstructure of 09G2S steel samples under different conditions: (a) base metal as delivered; (b) base metal after overheating; (c) weld metal as delivered; and (d) weld metal after overheating.

Overheating with slow cooling in the furnace formed a normalized ferrite–pearlite structure with a much larger grain (Figure 2b,d), where the pearlite was located mainly along the boundaries and in triple junctions of ferrite grains. In addition, overheating led to the appearance of a pronounced inequigranularity. The ferrite grain size in the weld metal was smaller than in the base metal. The grain size of the former austenite was also smaller in the weld metal than in the base metal.

The TEM analysis made it possible to detail the microstructure of the samples. Figure 3 shows the TEM images of the microstructure of the base metal samples in the as-delivered condition and after overheating. In the structure of the base metal samples in the as-delivered condition, an increased density of dislocations was observed. Some grains were fragmented into bands several hundred micrometers wide, which were the decomposition products of lower bainite. In addition, oval or irregularly shaped particles ranging in size from 50 to 500 nm were found in the structure. The particles were located both in the body of the grain and along the boundaries. The distribution of particles in the structure was nonuniform. The EDS analysis in the mapping mode showed that these particles were manganese carbides (Figure 4). Many particles were also enriched with iron; this indicates that some of the manganese atoms in the carbide were replaced by iron atoms. After overheating the base metal in the as-delivered condition, the grain coarsened and a pearlite component appeared in the structure, formed by parallel thin (25–50 nm) plates of iron and manganese carbides located in the body of the grain.

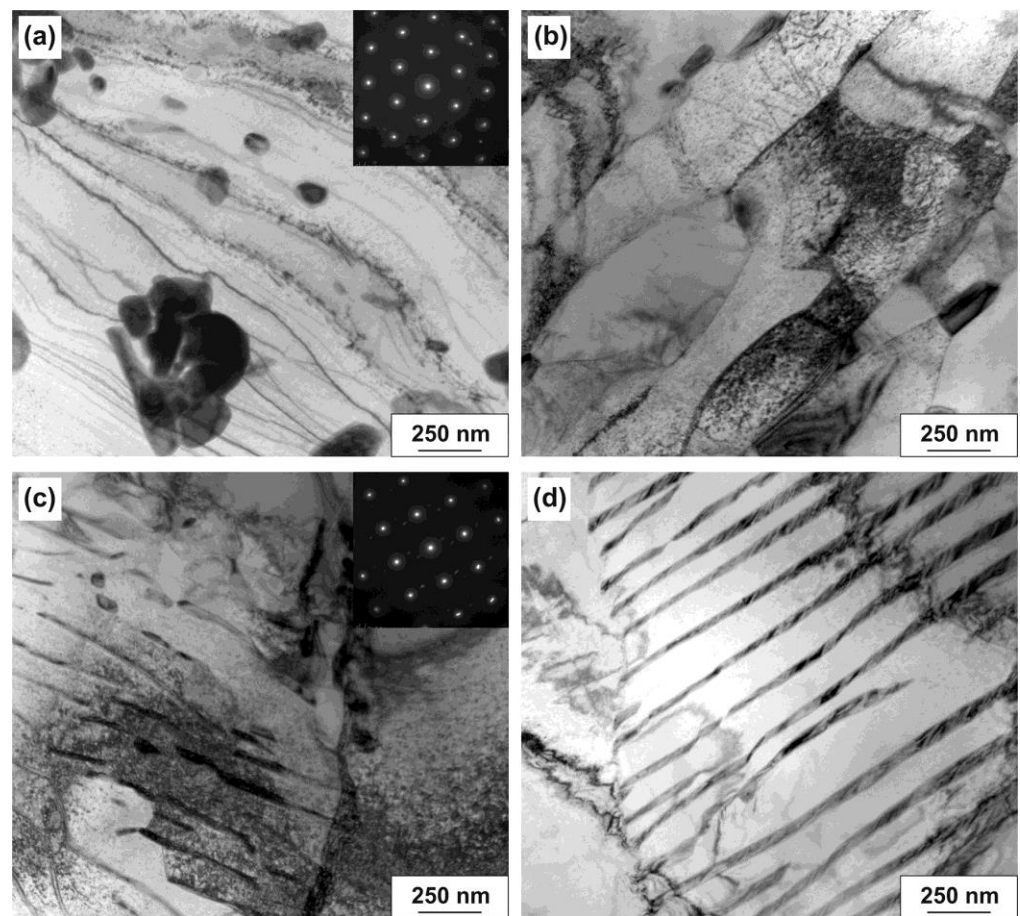


Figure 3. TEM microstructure of the base metal (a,b) as delivered and (c,d) after overheating.

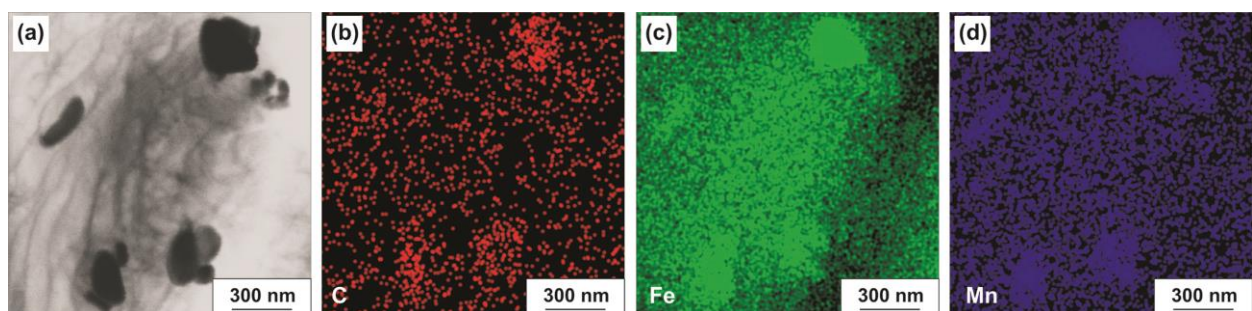


Figure 4. (a) Microstructure images and (b,c,d) EDS results of the base metal as delivered.

Figure 5 shows the TEM images of the microstructure of the weld metal samples as delivered and after overheating. The main difference between the structure of the weld metal and the base metal in the as-delivered condition was that a large number of particles were located along the grain boundaries in the weld metal. The particle size was the same as in the base metal, ranging from 50 to 500 nm. The structure mainly contained manganese carbides enriched with iron. Manganese sulfides were also found (Figure 6). These particles effectively inhibited grain growth; the consequence of this was a fine-grained structure of the weld. In addition, groups of very small grains of 0.5–1.0 μm in size, surrounded by particles, were revealed in the structure against a background of larger grains. After overheating, the microstructure of the weld was similar to the microstructure of the base metal; however, the carbide plates were rougher and more inhomogeneous.

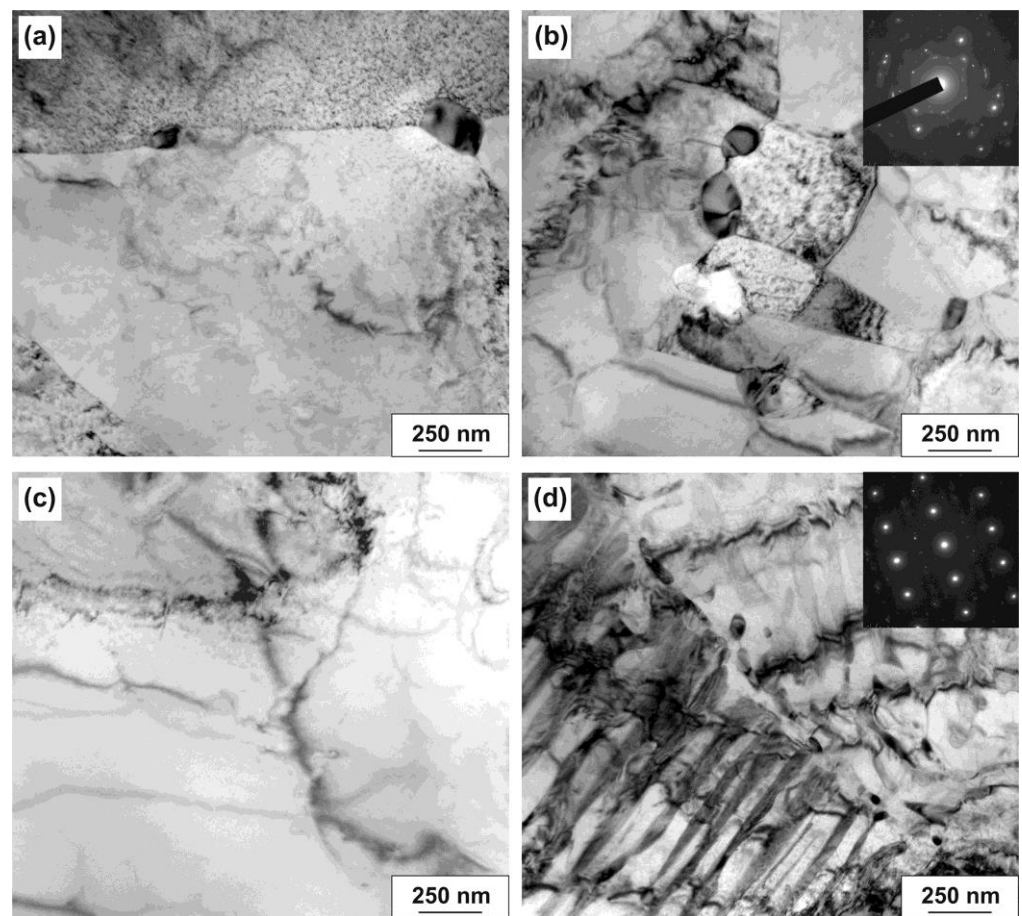


Figure 5. TEM microstructure of the weld metal (a,b) as delivered and (c,d) after overheating.

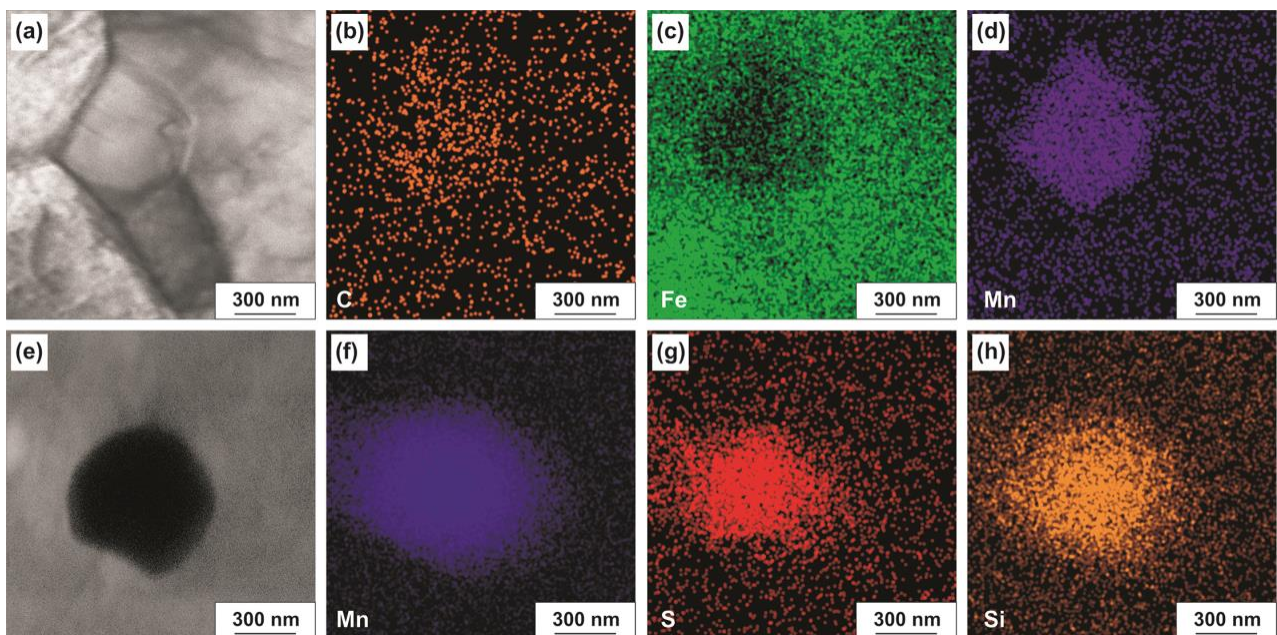


Figure 6. (a,e) Microstructure images and (b–d,f–h) EDS results of the weld metal as delivered.

3.2. Mechanical Properties

Table 2 shows the mechanical properties of the 09G2S steel samples under four conditions, which were obtained by testing for static tension and fatigue. The samples of the base metal and weld metal as delivered had comparable static mechanical properties; the strength of the base metal samples was only 8% higher than the strength of the weld metal. Overheating led to a decrease in the strength (especially the yield strength) and an increase in the relative elongation as a result of grain growth. The relative effect of overheating on the reduction in the yield strength of the base metal and the weld metal was comparable (about 20%). The room temperature impact toughness (KCV) was 355, 377, 144, and 143 J/cm², respectively, for the materials in the following order: base metal, base metal after overheating, weld metal, and weld metal after overheating [13].

Table 2. Mechanical properties of 09G2S steel samples under different conditions.

Material, Processing	Yield Strength, MPa	Tensile Strength, MPa	Elongation, %	Endurance Limit, MPa	Ratio of Endurance Limit to Tensile Strength
Base metal, as delivered	430 ± 15	556 ± 12	28 ± 2	475	0.9
Weld metal, as delivered	377 ± 23	507 ± 21	30 ± 3	420	0.8
Base metal, overheated	319 ± 7	511 ± 7	35 ± 2	385	0.7
Weld metal, overheated	305 ± 14	461 ± 6	43 ± 2	390	0.8

The microhardness profiles across the welded joint are shown in Figure 7. The averaged microhardness of the weld metal as delivered was 182 ± 7 HV, and after overheating, it decreased to 152 ± 8 HV. The microhardness of the base metal as delivered was 199 ± 4 HV, and after overheating, it decreased to 170 ± 11 HV. Thus, overheating led to a decrease in the microhardness of both the base metal and the weld metal by 15%. The decrease in the microhardness values of the steel after overheating was correlated with its tensile strength.

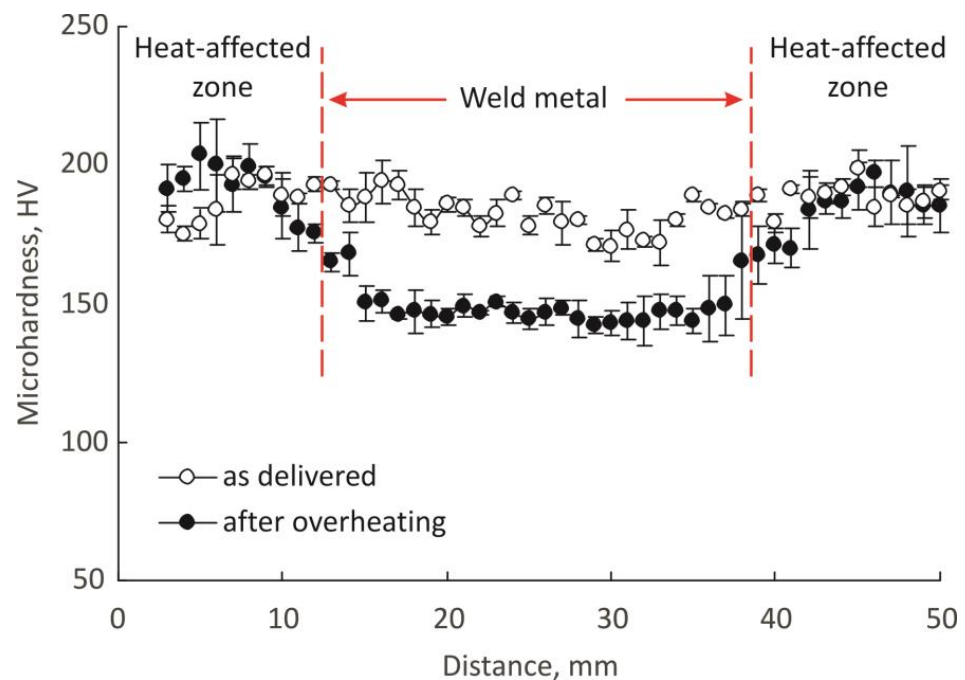


Figure 7. The welded joint microhardness profiles before and after overheating.

Figure 8 shows the curves of the “maximum cycle stress—number of cycles to failure” in semi-logarithmic coordinates for the 09G2S steel samples under four conditions.

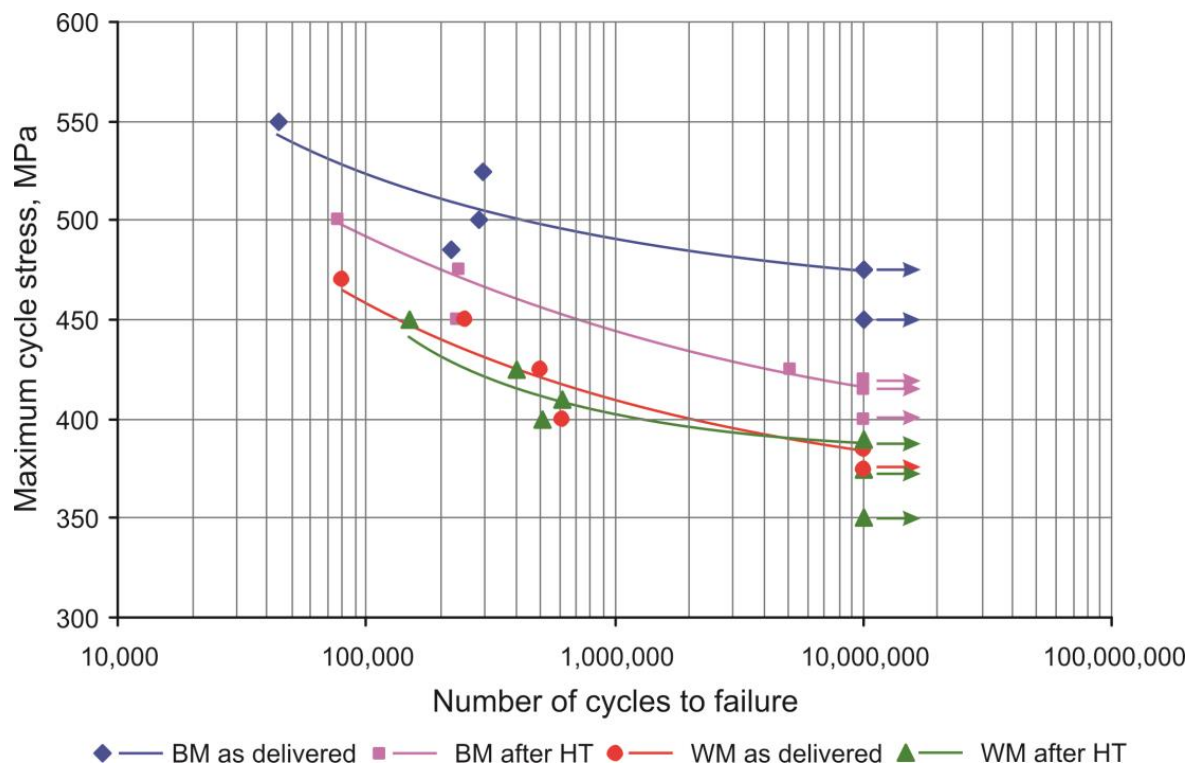


Figure 8. Fatigue curves for 09G2S steel samples under different conditions: BM—base metal; WM—weld metal; HT—overheating. The non-failed specimens are marked with arrows.

The samples of the base metal as delivered were characterized by the highest endurance limit of 475 MPa. The samples of the weld metal as delivered had a 12% lower endurance limit. Overheating led to a decrease in the endurance limit of the base metal samples by 19% and the weld metal samples by 7%. After overheating, the endurance limit was comparable for the base metal samples and the weld metal samples.

3.3. Fractographic Analysis

Figure 9 shows the SEM images of the fractures' surfaces in the base metal specimens as delivered and after overheating; Figure 10 shows the SEM images of the fractures' surfaces in the weld metal as delivered and after overheating. The fractures' surfaces for all specimens had a typical fatigue structure. At one of the side edges of the gauge part of the specimen, there was a fatigue crack initiation zone. Furthermore, the crack propagated in a fan shape deep into the specimen. The fatigue crack propagation zone was replaced by a static rupture. The area of the fatigue failure was small in relation to the cross-sectional area of the specimen (by a factor of 5–20). As usual, as the cycle amplitude increased, the area of the fatigue failure decreased.

The fractures' surfaces in the base metal specimens as delivered are shown on a micro level in Figure 11. The fatigue crack propagation zone was flat and the fracture mechanism was quasi-brittle. Very thin (0.5 μm) brittle fatigue micro-grooves are present. The grooves were discontinuous, and their presence in the fracture was irregular. In the fractures of the specimens tested at a high cycle amplitude, grooves were rarely detected. The static rupture of the specimen occurred entirely through a finely dimpled ductile mechanism.

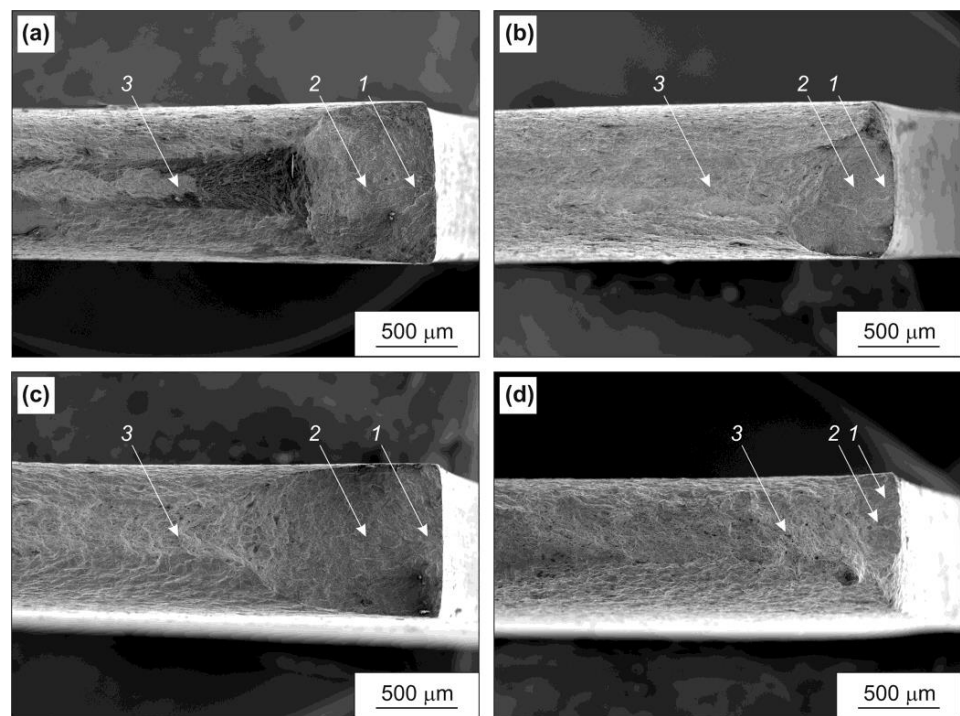


Figure 9. General view of the fatigue fractures' surfaces in the base metal. (1) Fatigue crack initiation zone; (2) fatigue crack propagation zone; and (3) static rupture zone. (a) As delivered, with a low cycle amplitude; (b) as delivered, with a high cycle amplitude; (c) after overheating, with a low cycle amplitude; and (d) after overheating, with a high cycle amplitude.

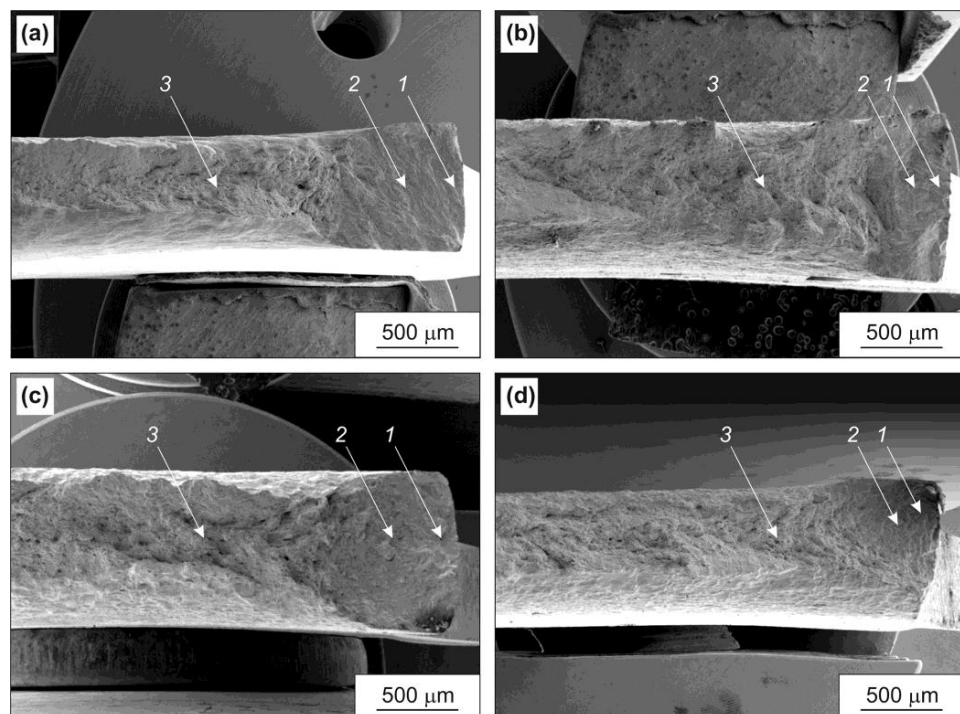


Figure 10. General view of the fatigue fractures' surfaces in the weld metal. (1) Fatigue crack initiation zone; (2) fatigue crack propagation zone; and (3) static rupture zone. (a) As delivered, with a low cycle amplitude; (b) as delivered, with a high cycle amplitude; (c) after overheating, with a low cycle amplitude; and (d) after overheating, with a high cycle amplitude.

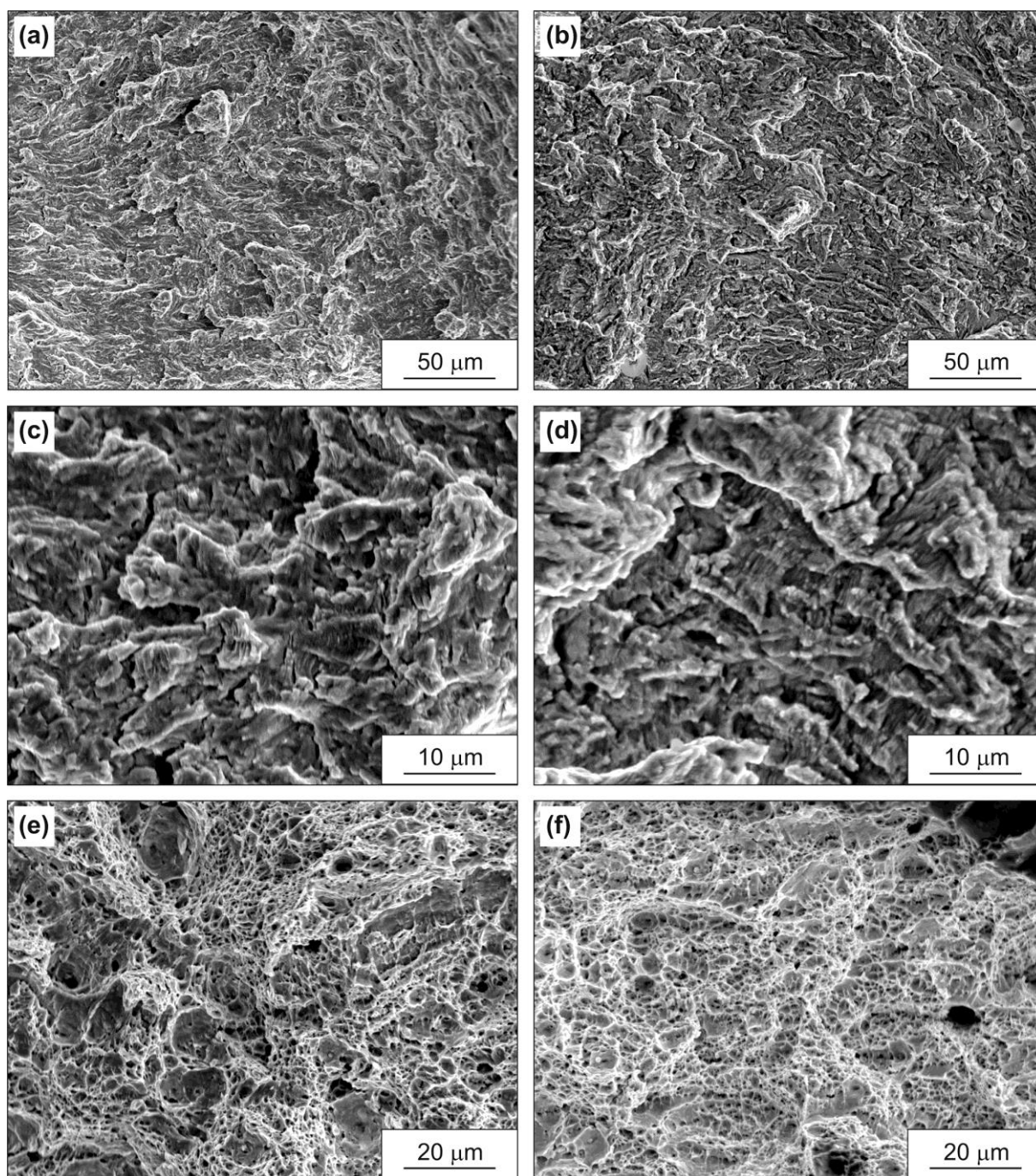


Figure 11. The fatigue fractures' surfaces in the base metal as delivered, shown on a micro level: (a,c,e) with a high cycle amplitude; (b,d,f) with a low cycle amplitude.

The fractures' surfaces in the base metal specimens after overheating are shown on a micro level in Figure 12. After overheating, the fatigue crack propagation zone had a more pronounced relief. It is clear that the formation of the relief was associated with plastic deformation. In turn, external energy was required to develop the plastic deformation. Therefore, a more developed relief indicated more energy expended on the fracture process. The crack propagated with the formation of numerous parallel micro-grooves, in which the distance between grooves was 0.5 μm. In the fractures of specimens tested at a high cycle amplitude, grooves were found less frequently. The static rupture of the specimen occurred entirely through a finely dimpled ductile mechanism, but the size of the dimples was an order of magnitude larger than in the fractures of the specimens as delivered.

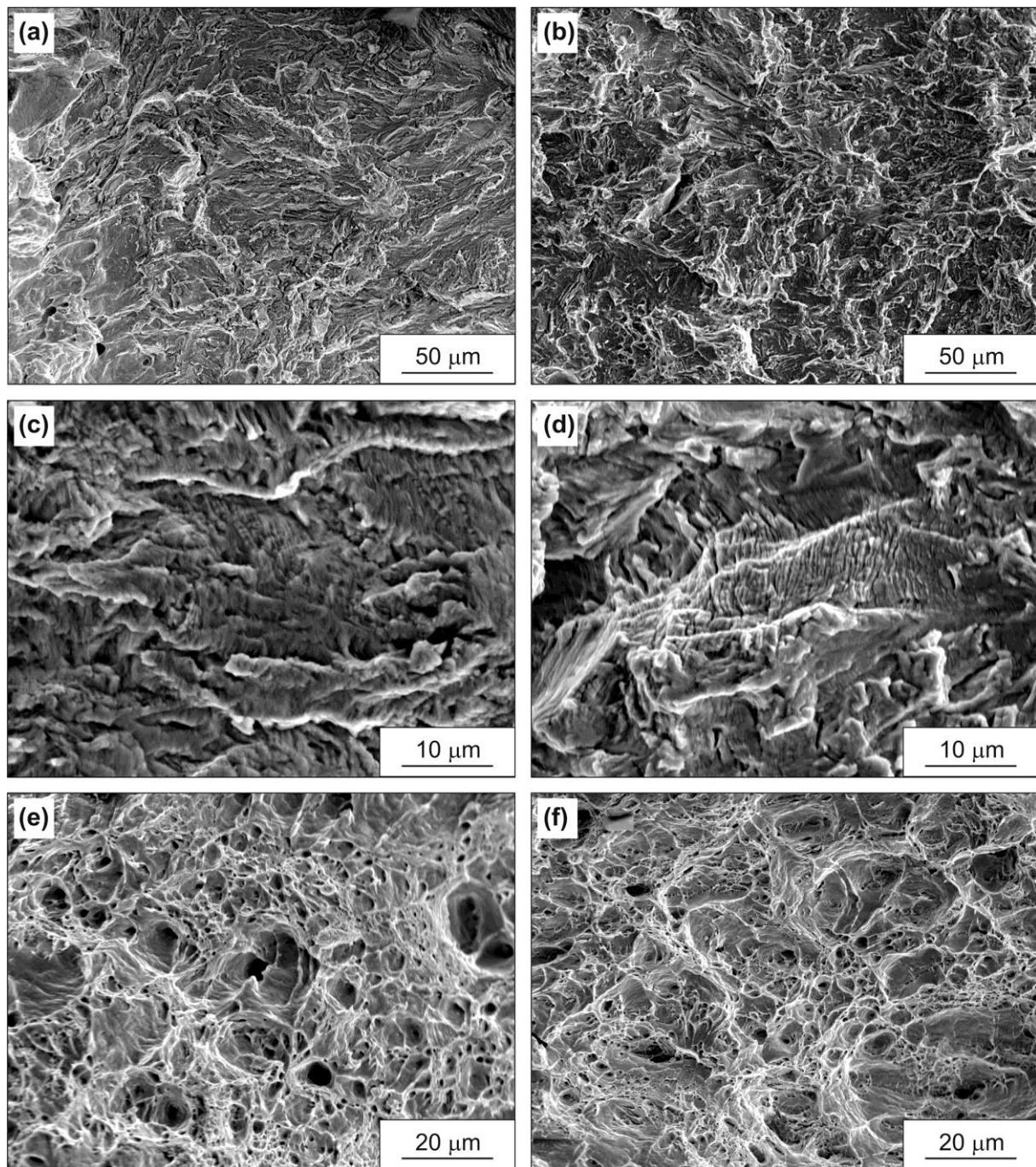


Figure 12. The fatigue fractures' surfaces of the base metal after overheating, shown on a micro level: (a,c,e) with a high cycle amplitude; (b,d,f) with a low cycle amplitude.

The fractures' surfaces in the weld metal specimens as delivered are shown on a micro level in Figure 13, and they are shown after overheating in Figure 14. On a micro level, the fractures in the weld metal specimens as delivered were similar to the fractures in the base metal after overheating. The fractures in the weld metal specimens after overheating were of a similar type.

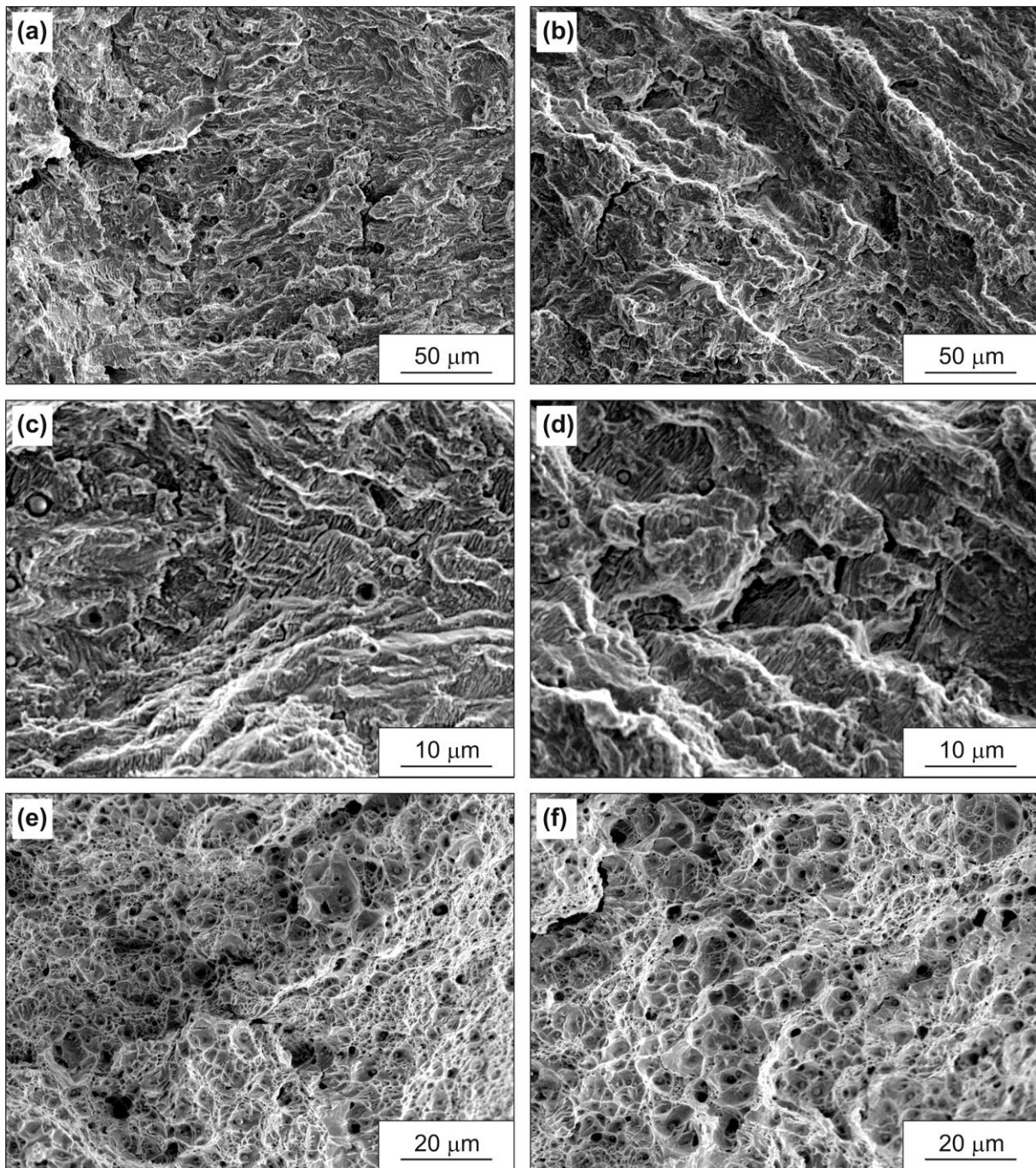


Figure 13. The fatigue fractures' surfaces in the weld metal as delivered, shown on a micro level: (a,c,e) with a high cycle amplitude; (b,d,f) with a low cycle amplitude.

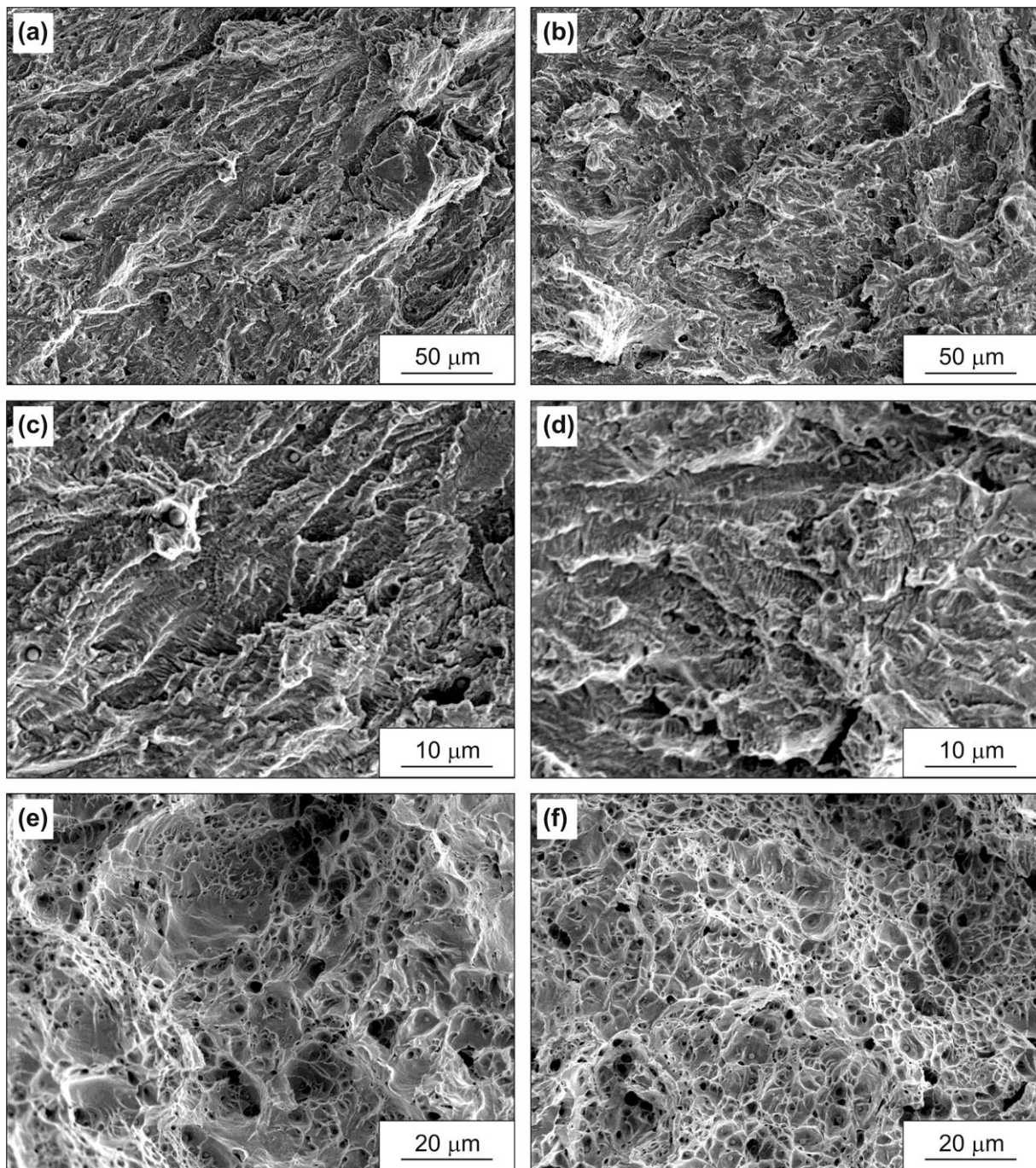


Figure 14. The fatigue fractures' surfaces in the weld metal after overheating, shown on a micro level: (a,c,e) with a high cycle amplitude; (b,d,f) with a low cycle amplitude.

The propagation of fatigue cracks occurred with secondary branching and with a large plastic deformation at the crack tip. During fatigue testing, a deformation relief was found on the polished surface of the gauge part of the specimen, formed by numerous zones of plastic deformation (Figure 15). As the cycle amplitude increased, numerous parallel slip bands formed on the specimen's surface (Figure 16). The distance between adjacent secondary cracks was greater than the average grain size. This indicates that most of the secondary cracks propagated along the boundaries of a group of several grains. The average distance between adjacent secondary cracks on the specimens' surfaces was greater for the specimens after overheating than for the specimens as delivered.

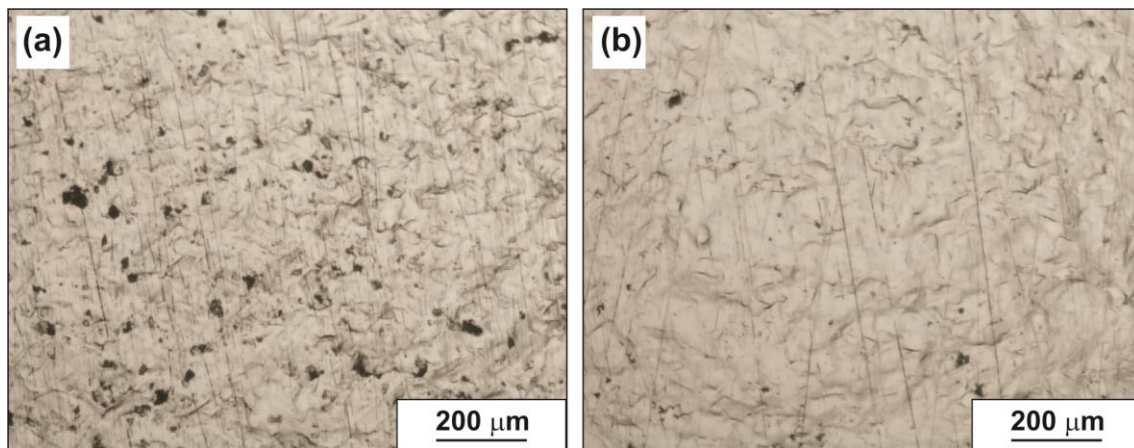


Figure 15. Deformation relief on the gauge part's surface for the (a) overheated base metal specimen and (b) overheated weld metal specimen after fatigue tests below the endurance limit.

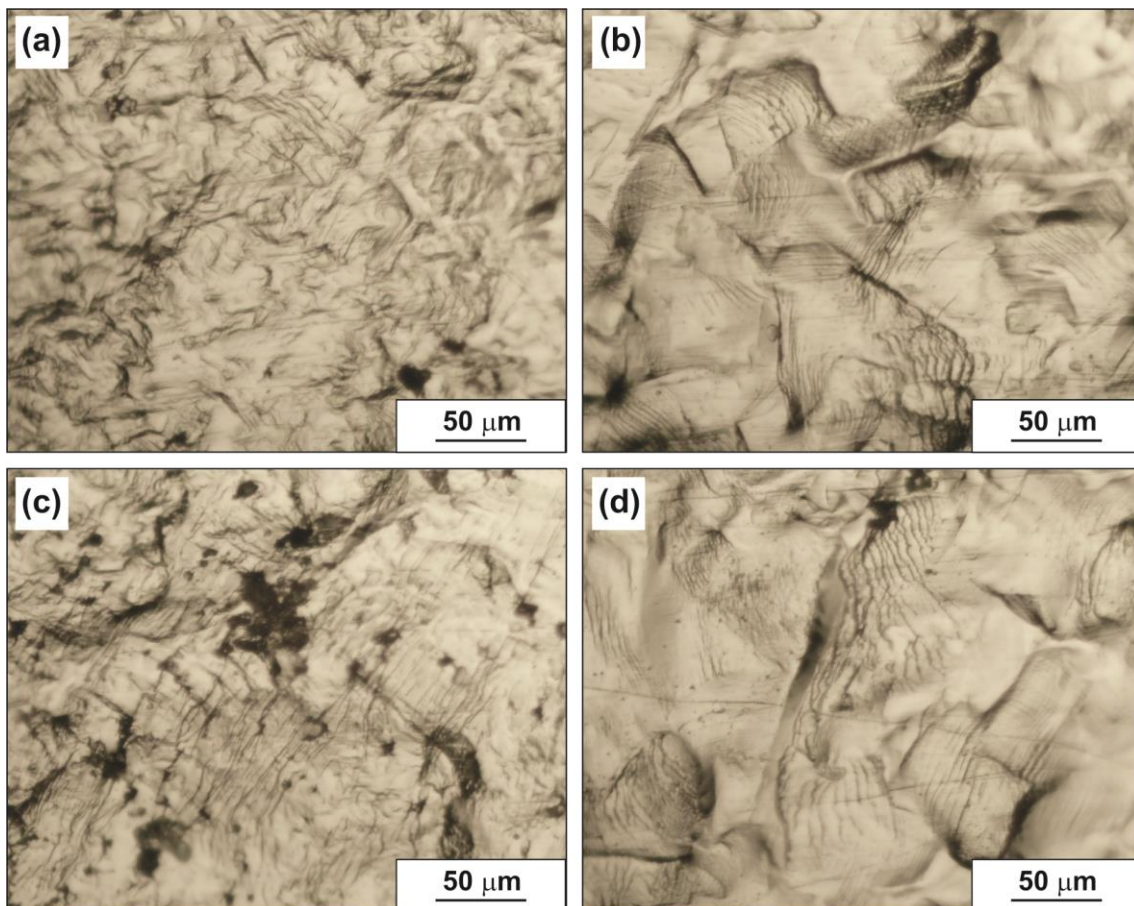


Figure 16. Deformation relief on the gauge part's surface for the (a,b) base metal specimen and (c,d) weld metal specimen after fatigue tests above the endurance limit: (a,c) in the as-delivered condition; (b,d) after overheating.

4. Discussion

According to the results obtained, the base metal as delivered had a high resistance to fatigue failure—the endurance limit was 90% of the tensile strength. It is interesting to note that the endurance limit was 19% higher than the static yield strength. This was due to the cyclic hardening of the samples during testing, which is typical for low-carbon

steels [19]. The phenomenon of cyclic hardening usually refers to low-cycle fatigue, which is when the material is loaded in the plastic deformation region [30]. However, in our case, the entire range of cycle stresses was above the static yield strength of the steel; thus, fatigue loading was carried out precisely in the plastic deformation region. The hardening of low-carbon steel above the static yield stress during cyclic loading has been previously observed [14,25]. For 09G2S steel samples under other conditions, the endurance limit was also higher than their static yield strength. Thus, during testing, the samples of all conditions demonstrated cyclic hardening. These results differ from those obtained in [31] for steel of a similar chemical composition but with a ferrite–pearlite structure, for which the fatigue limit up to 10^7 cycles was below the static yield strength.

The presence of fine particles of carbides in the steel structure refined the grain, which had a positive effect on the static and cyclic strength of both the base metal and the weld metal.

The cyclic strength of the samples correlated well with the fatigue fracture mechanism. Therefore, with the highest fatigue life, the base metal as delivered had the least ductile character of fatigue crack propagation. This was due to the significant hardening of the metal during cyclic loading.

Overheating caused a decrease not only in the static strength (primarily in the yield strength) but also in the cyclic strength. This was due to the influence of the microstructure on the fracture toughness of the material which, in turn, affected the rate of fatigue crack propagation. The rough periodic structure of overheating metal with extended carbide plates reduced the toughness of the material. When a fatigue crack propagated, the cleavage of the carbide particles occurred, which led to an increase in the fatigue crack growth rate. It is well known that the rate of fatigue crack propagation is higher for a lamellar pearlite structure than for a spheroidized one [32]. However, considering that 09G2S steel contains only 0.1% carbon, the total fraction of carbides in the steel structure is small (no more than 2%). Therefore, steel in an overheated condition retains the ability to cyclically harden; at the same time, however, the tendency of the metal to cyclically harden weakens, and micro-grooves in the fatigue crack propagation zone become more pronounced.

Thus, the base metal and the weld metal after high-temperature exposure had a comparable static yield strength and endurance limit, which is explained by their similar structure. At the same time, the previously obtained values of the impact toughness of the base metal and weld metal did not correlate with their structure [13], and this issue requires further in-depth study.

The results of this study confirm the high resistance to fatigue failure of the CC vessel's structural elements, both under operating conditions and after the thermal effects typical of severe accidents beyond the design basis. Although the object of this study was the weld itself, at the same time, the fusion zone and heat-affected zone are potential weak points in the welded joint. On the contrary, no negative effects on the fatigue strength of these zones were noted in a number of papers. Regardless, it will be useful to study the fatigue strength of the fusion zone and heat-affected zone in the future. In addition, an analysis of weld defects and the use of predictive fatigue life models can be considered as another direction for further research [26,27].

5. Conclusions

According to the results of the high-cycle fatigue tests for the base metal and weld metal (automatic argon arc welding) of 09G2S steel before and after overheating while simulating the conditions of an accident beyond the design basis at a nuclear power plant (1200 °C, 3.7 h), the following results were established:

- (1) The samples under all conditions had a high endurance limit, which was 70–90% of the ultimate strength. The highest endurance limit of the base metal samples as delivered was 475 MPa. The endurance limit of the weld metal samples as delivered was lower by 12%. Overheating led to a decrease in the endurance limit of the base metal samples by 19% and in the weld metal samples by 7%.

- (2) During fatigue testing, all samples showed cyclic hardening behavior.
- (3) The mechanism of fatigue fractures for all samples was quasi-brittle with the presence of very thin fatigue micro-grooves.

Author Contributions: Conceptualization, S.A.N.; methodology, V.A.B. and D.V.P.; investigation, S.O.R., S.V.P., N.V.S., M.Y.Z. and V.M.K.; writing—original draft preparation, S.O.R.; writing—review and editing, S.A.N.; visualization, D.V.P., M.Y.Z. and V.M.K. All authors have read and agreed to the published version of the manuscript.

Funding: This research received no external funding.

Institutional Review Board Statement: Not applicable.

Informed Consent Statement: Not applicable.

Data Availability Statement: The raw/processed data required to reproduce these findings cannot be shared at this time as the data also form part of an ongoing study.

Conflicts of Interest: The authors declare no conflict of interest.

References

1. DIN 17145-80; Round Wire Rod for Welding Filler Metals. Technical Conditions of Delivery; Beuth Publishing: Berlin, Germany, 1980.
2. Budynas, R.G.; Nisbett, J.K. *Shigley's Mechanical Engineering Design*, 9th ed.; McGraw-Hill: New York, NY, USA, 2011; pp. 49–52.
3. Kuptsov, S.G.; Pleshchev, V.P.; Magomedova, R.S.; Nikonenko, E.A.; Shimov, V.V. Hybrid Hardening of Structural Steel, Grade 09G2S. *Steel Transl.* **2021**, *51*, 342–344. [[CrossRef](#)]
4. Kryukov, R.E.; Gromov, V.E.; Ivanov, Y.F.; Kozyrev, N.A.; Rubannikova, Y.A. Fine Structure and Fracture Surface of Low-Carbon Steel Welds. *Russ. Phys. J.* **2021**, *65*, 332–336. [[CrossRef](#)]
5. Saraev, Y.N.; Gladkovsky, S.V.; Lepikhin, S.V.; Dvoynikov, D.A.; Kamantsev, I.S.; Veselova, V.E. Influence of the welding method on the impact strength and cyclic fracture toughness parameters of the 09G2S steel. *AIP Conf. Proc.* **2017**, *1915*, 030024. [[CrossRef](#)]
6. Vorontsov, A.V.; Utyaganova, V.R.; Chumaevskii, A.V.; Gurianov, D.A.; Ivanov, A.N. Structure and mechanical properties of laser-arc hybrid welding of 13Mn6 steel welded with austenitic filler. *IOP Conf. Ser. Mater. Sci. Eng.* **2019**, *537*, 022071. [[CrossRef](#)]
7. Khadeev, G.E. Effect of Multistage Deformation during the Pipe Manufacturing on Mechanical Properties of Steels Strength Grade X70–X80. *Key Eng. Mater.* **2016**, *716*, 957–962. [[CrossRef](#)]
8. Odesskii, P.D.; Egorova, A.A. Strength of steel for unique engineering structures. *Russ. Metall.* **2012**, *2012*, 911–918. [[CrossRef](#)]
9. Nikulin, S.A.; Rogachev, S.O.; Belov, V.A.; Turilina, V.Y.; Shplis, N.V. Effect of High Temperatures on the Mechanical Properties of the Weld Metal in the Welded Joint of Low-Carbon Low-Alloy Steel. *Russ. Metall.* **2021**, *2021*, 1314–1319. [[CrossRef](#)]
10. Fischer, M. The severe accident mitigation concept and the design measures for core melt retention of the European Pressurized Reactor (EPR). *Nucl. Eng. Des.* **2004**, *230*, 169–180. [[CrossRef](#)]
11. Sultan, T.; Sapra, M.K.; Kundu, S.; Kadam, A.V.; Kulkarni, P.P.; Rao, A.R. Experimental & analytical study of passive thermal sensing system developed for cooling water injection into AHWR core catcher. *Nucl. Eng. Des.* **2017**, *322*, 81–91. [[CrossRef](#)]
12. Chen, C.Y.; Huang, J.Y.; Yeh, J.J.; Hwang, J.R.; Huang, J.Y. Microstructural evaluation of fatigue damage in SA533-B1 and type 316L stainless steels. *J. Mater. Sci.* **2003**, *38*, 817–822. [[CrossRef](#)]
13. Nikulin, S.A.; Rogachev, S.O.; Belov, V.A.; Komissarov, A.A.; Turilina, V.Y.; Shplis, N.V.; Nikolaev, Y.A. Impact strength of low-carbon steel 09G2S welded joint metal. *Metallurgist* **2022**, *65*, 1391–14009. [[CrossRef](#)]
14. Kim, Y.; Hwang, W. High-Cycle, Low-Cycle, Extremely Low-Cycle Fatigue and Monotonic Fracture Behaviors of Low-Carbon Steel and Its Welded Joint. *Materials* **2019**, *12*, 4111. [[CrossRef](#)] [[PubMed](#)]
15. Hasunuma, S.; Oki, S.; Motomatsu, K.; Ogawa, T. Fatigue life prediction of carbon steel with machined surface layer under low-cycle fatigue. *Int. J. Fatigue* **2019**, *123*, 255–267. [[CrossRef](#)]
16. Huang, Z.Y.; Wagner, D.; Bathias, C.; Chaboche, J.L. Cumulative fatigue damage in low cycle fatigue and gigacycle fatigue for low carbon–manganese steel. *Int. J. Fatigue* **2011**, *33*, 115–121. [[CrossRef](#)]
17. Zhou, Q.; Qian, L.; Meng, J.; Zhao, L.; Zhang, F. Low-cycle fatigue behavior and microstructural evolution in a low-carbon carbide-free bainitic steel. *Mater. Des.* **2015**, *85*, 487–496. [[CrossRef](#)]
18. Rosado-Carrasco, J.G.; González-Zapatero, W.F.; García, C.J.; Gómora, C.M.; Jaramillo, D.; Ambriz, R.R. Analysis of the Low Cycle Fatigue Behavior of DP980 Steel Gas Metal ArcWelded Joints. *Metals* **2022**, *12*, 419. [[CrossRef](#)]
19. Nip, K.H.; Gardner, L.; Davies, C.M.; Elghazouli, A.Y. Extremely low cycle fatigue tests on structural carbon steel and stainless steel. *J. Constr. Steel. Res.* **2010**, *66*, 96–110. [[CrossRef](#)]
20. Zhang, M.; Yang, P.; Tan, Y. Micromechanisms of fatigue crack nucleation and short crack growth in a low carbon steel under low cycle impact fatigue loading. *Int. J. Fatigue* **1999**, *21*, 823–830. [[CrossRef](#)]
21. Prosvirnin, D.V.; Kolmakov, A.G.; Larionov, M.D.; Pivovarchik, S.V. Peculiarities of deformation of thin-sheet TRIP steel under static and fatigue loading. *J. Phys. Conf. Ser.* **2021**, *1758*, 012042. [[CrossRef](#)]

22. Plumbridge, W.J. Review: Fatigue-crack propagation in metallic and polymeric materials. *J. Mater. Sci.* **1972**, *7*, 939–962. [[CrossRef](#)]
23. Masuda, C.; Ohta, A.; Nishijima, S.; Sasaki, E. Fatigue striation in a wide range of crack propagation rates up to 70 $\mu\text{m}/\text{cycle}$ in a ductile structural steel. *J. Mater. Sci.* **1980**, *15*, 1663–1670. [[CrossRef](#)]
24. Gjonaj, M.; Cukalla, M. High cycle fatigue of low alloy carbon steels. *J. Mater. Process. Technol.* **1997**, *64*, 141–148. [[CrossRef](#)]
25. Botvina, L.R.; Petrova, I.M.; Gadolina, I.V.; Levin, V.P.; Demina, Y.A.; Soldatenkov, A.P.; T'utin, M.P. High-Cycle Fatigue Failure of Low-Carbon Steel after Long-Term Aging. *Inorg. Mater.* **2010**, *46*, 1570–1577. [[CrossRef](#)]
26. He, J.-C.; Zhu, S.-P.; Luo, C.; Niu, X.; Wang, Q. Size effect in fatigue modelling of defective materials: Application of the calibrated weakest-link theory. *Int. J. Fatigue.* **2022**, *165*, 107213. [[CrossRef](#)]
27. Liao, D.; Zhu, S.-P.; Keshtegar, B.; Qian, G.; Wang, Q. Probabilistic framework for fatigue life assessment of notched components under size effects. *Int. J. Mech. Sci.* **2020**, *181*, 105685. [[CrossRef](#)]
28. GOST 25.502-79; Strength Analysis and Testing in Machine Building. Methods of Metals Mechanical Testing. Methods of Fatigue Testing. GostPerevod: Moscow, Russia, 1979.
29. Pumpyanskiy, D.A.; Pyshmintcev, I.Y.; Maltseva, A.N.; Khatkevich, V.M.; Arsenkin, A.M. Strain Hardening of 09G2S Steel at Elevated Temperatures. *Russ. Metall.* **2021**, *2021*, 1128–1134. [[CrossRef](#)]
30. Noh, K.; Shams, S.A.A.; Kim, W.; Kim, J.N.; Lee, C.S. Influence of Microstructure on Low-Cycle and Extremely-Low-Cycle Fatigue Resistance of Low-Carbon Steels. *Met. Mater. Int.* **2021**, *27*, 3862–3874. [[CrossRef](#)]
31. Kim, Y.; Kwon, J.; Lee, H.; Jang, W.; Choi, J.; Kim, S. Effect of Microstructure on Fatigue Crack Propagation and S–N Fatigue Behaviors of TMCP Steels with Yield Strengths of Approximately 450 MPa. *Metall. Mater. Trans. A* **2011**, *42*, 986–999. [[CrossRef](#)]
32. Heald, P.T.; Lindley, T.C.; Richards, C.E. The influence of stress intensity and microstructure on fatigue crack propagation in a 1% carbon steel. *Mater. Sci. Eng.* **1972**, *10*, 235–240. [[CrossRef](#)]

Disclaimer/Publisher's Note: The statements, opinions and data contained in all publications are solely those of the individual author(s) and contributor(s) and not of MDPI and/or the editor(s). MDPI and/or the editor(s) disclaim responsibility for any injury to people or property resulting from any ideas, methods, instructions or products referred to in the content.